

A spectrally discretized wide-angle parabolic equation model for simulating acoustic propagation in laterally inhomogeneous oceans

Houwang Tu,¹  Yongxian Wang,^{2,a)}  Yinuo Zhang,²  Xiaodong Wang,¹ and Wei Liu² 

¹College of Computer, National University of Defense Technology, Changsha, 410073, China

²College of Meteorology and Oceanography, National University of Defense Technology, Changsha, 410073, China

ABSTRACT:

Sound waves can be used to carry out underwater activities. Rapidly and accurately simulating sound propagation is the basis for underwater detection. The wide-angle parabolic model has a good computational speed and accuracy and is currently the main numerical model for mid- and low-frequency sound propagation. The classical wide-angle parabolic equation model is discretized by the finite difference method and a low-order difference scheme is generally adopted. In this paper, a wide-angle parabolic equation model based on a spectral method is proposed. The depth operators of each layer are discretized via the Chebyshev spectral method and then assembled into a global matrix for the forward step. Lateral inhomogeneity is addressed by updating the global depth matrix while stepping forward. In the proposed spectral algorithm, both soft and hard seabeds can be accurately simulated by imposing boundary conditions, and the perfectly matched layer technique is used to truncate the unbounded acoustic half-space. Several representative numerical experiments prove the accuracy and efficiency of the proposed algorithm. However, the spectral method requires that the thickness of the layers does not change during the forward step. Thus, the current spectral algorithm cannot simulate waveguides with terrain undulation, which is its main limitation.

© 2023 Acoustical Society of America. <https://doi.org/10.1121/10.0019748>

(Received 10 February 2023; revised 1 June 2023; accepted 2 June 2023; published online 16 June 2023)

[Editor: Nicholas P. Chotiros]

Pages: 3334–3349

I. INTRODUCTION

Sound propagation in the ocean is a crucial topic in ocean acoustics.¹ In recent decades, the development of numerical algorithms and scientific computing platforms has contributed to remarkable achievements in ocean acoustics and contributed to the gradual formation of a new subdiscipline, computational ocean acoustics.² In linear acoustics, frequency-domain sound propagation satisfies the Helmholtz equation. The essence of computational ocean acoustics is to solve the Helmholtz equation with various boundary conditions and in various ocean acoustic environments. The Helmholtz equation is an elliptic equation that is computationally expensive to solve directly, thus making its practical application difficult. To reduce the computational cost, researchers have developed ray models, wavenumber integration models, normal mode models, and parabolic equation (PE) models. Each of these models has its own applicability and limitations and has made useful contributions to ocean acoustic simulations.^{1–3}

PE models have undergone rapid development since their introduction into ocean acoustics because of their good balance between computational speed and accuracy and are currently among the most commonly used models for low- and mid-frequency underwater acoustic simulation. The PE

approach was initially extended to ocean acoustics from the radio field in 1977 by Tappert,⁴ the standard PE model and “split-step” Fourier algorithm were proposed by Hardin and Tappert.^{4,5} At this time, PE models were only suitable for narrow-angle sound propagation. Later, many scholars devoted themselves to studying the coefficients of operator approximation to expand the applicable range of sound propagation angles for PE models.^{6–8}

In 1989, Collins applied Galerkin’s method to discretize the radical operator and proposed a higher-order elastic PE for calculating sound propagation in elastic media.⁹ He then applied the theory of an energy-conserving correction¹⁰ and the rational approximation of the Padé series to eliminate Gibbs oscillations, thereby developing a stable higher-order energy-conserving PE.^{11–13} The high-order Padé approximation enables the PE to handle propagation angles of up to almost 90°, and the “split-step” format greatly accelerates the computation, thus providing a better solution for scenarios with range-dependent ocean depth, sound speed, and density.^{14,15} In early PE modeling studies, the initial field was obtained based on the normal modes and a Gaussian initial field. In 1992, Collins successfully introduced a self-starter for the PE models for a field excited by a sound source in a fluid medium.¹⁶ Because the seabeds in offshore areas mostly consist of wedge-shaped seamounts and other variable broken-line media, it is necessary to be able to properly handle an inclined seabed boundary. Collins used

^{a)}Electronic mail: yxwang@nudt.edu.cn

the coordinate rotation method to solve the PE model for an inclined seabed boundary and then solved the energy-loss problem caused by stepwise approximation through energy-conserving approximation.¹⁷ Another commonly used method for addressing inclined seafloors is the coordinate mapping method.^{18,19} Collins made several important contributions to the development of the PE method. He developed the RAM series of underwater acoustic numerical models based on his research achievements, including RAM, RAMS, RAMSurf, and RAMGeo.²⁰ Currently, these models are the most advanced and widely used PE models in the field of ocean acoustics. In RAM, the depth operator is discretized by means of the finite difference method based on the Galerkin method, and the linear equations are solved via the Gaussian elimination method of bidirectional scanning.²¹

In the context of numerical methods, spectral methods have begun to gain popularity in computational ocean acoustics in recent years. Although spectral methods are still a niche class of numerical methods compared to the finite difference and finite element methods,^{22–24} their exponential error convergence is causing them to gradually gain prominence in scientific and engineering numerical simulations.^{25–27} The spectral approach was first introduced into the modeling of normal modes by Dzieciuch,^{28,29} and Evans subsequently developed the first mode solver for two-layer media.³⁰ Tu *et al.*^{31,32} and Sabatini *et al.*³³ developed three spectral methods to solve for the normal modes of horizontal multilayer media. Tu *et al.* conducted many numerical experiments using the numerical models they developed, and these experiments verified the correctness and high accuracy of spectral methods.^{34,35} In view of the advantages of spectral methods, Tu *et al.* further extended their application to coupled modes,^{36–38} adiabatic modes,³⁹ and wavenumber integration model.⁴⁰ Nevertheless, for PE models, the existing codes are still most commonly discretized by means of the finite difference method^{6,41–43} or the finite element method.^{44,45} Wang *et al.*⁴⁶ and Tu *et al.*⁴⁷ have made two preliminary attempts in this direction using two spectral methods and have proposed PE models for homogeneous media.^{48,49} However, these algorithms are only suitable for single-layer, range-independent waveguides and cannot be applied to simulate more complicated waveguides. In this paper, a Chebyshev–Tau spectral method is used to discretize the wide-angle PE model, and the applicability of the proposed spectral algorithm extends to multilayer media and laterally inhomogeneous waveguides.

II. THEORY AND MODEL

A. Wide-angle PE model

For the waveguide environment shown in Fig. 1, in the cylindrical coordinate system, the media are horizontally stratified, and the acoustic parameters are laterally inhomogeneous:

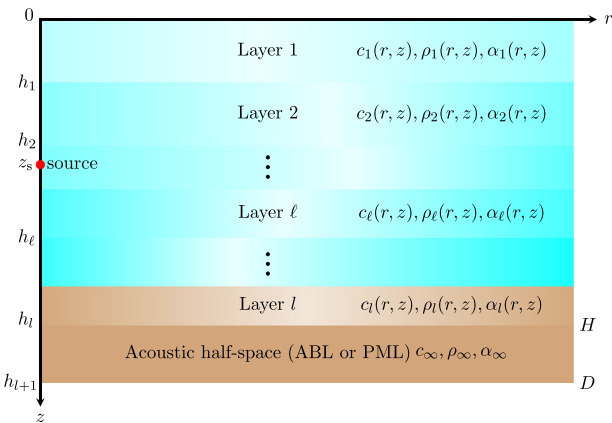


FIG. 1. (Color online) Schematic diagram of laterally inhomogeneous oceans.

$$c(r, z) = \begin{cases} c_\ell(r, z), & h_{\ell-1} \leq z \leq h_\ell, \\ c_\infty, & z \geq H, \end{cases} \quad (1a)$$

$$\rho(r, z) = \begin{cases} \rho_\ell(r, z), & h_{\ell-1} \leq z \leq h_\ell, \\ \rho_\infty, & z \geq H, \end{cases} \quad (1b)$$

$$\alpha(r, z) = \begin{cases} \alpha_\ell(r, z), & h_{\ell-1} \leq z \leq h_\ell, \\ \alpha_\infty, & z \geq H, \end{cases} \quad (1c)$$

where $c(r, z)$ is the sound speed of the media, $\rho(r, z)$ is the density of the media, $\alpha(r, z)$ is the attenuation coefficient, $h_0 = 0$, $h_l = H$, and $h_{l+1} = D$. There may be a homogeneous acoustic half-space below the depth H . The governing equation (a Helmholtz equation) of frequency-domain sound propagation is taken to be as follows:

$$\left[\frac{\partial^2}{\partial r^2} + \frac{1}{r} \frac{\partial}{\partial r} + \rho \frac{\partial}{\partial z} \left(\frac{1}{\rho} \frac{\partial}{\partial z} \right) + k^2 \right] P = 0, \quad (2)$$

where $P(r, z)$ is the frequency-domain sound pressure, $k(r, z) = 2\pi f/c(r, z)$ is the wavenumber, and f is the frequency of the acoustic source. In practice, to account for the effect of attenuation on sound propagation, k is usually considered to take the following form:

$$k(r, z) = \frac{2\pi f [1 + i\eta\alpha(r, z)]}{c(r, z)}, \quad \eta = \frac{1}{40\pi \log_{10} e}.$$

Notably that the sound propagation is cylindrical and can be replaced with the following variables:

$$p = \sqrt{r} P. \quad (3)$$

Then, the governing equation for p after the elimination of cylinder expansion can be written as follows:

$$\frac{\partial^2 p}{\partial r^2} + \rho \frac{\partial}{\partial z} \left(\frac{1}{\rho} \frac{\partial p}{\partial z} \right) + k^2 p + \frac{p}{4r^2} = 0. \quad (4)$$

Under the assumption that the main region of concern is the far field, the following equation can be obtained:

$$k^2 p \gg \frac{p}{4r^2}. \quad (5)$$

This indicates that $p/4r^2$ in Eq. (4) is negligible; therefore, we have

$$\frac{\partial^2 p}{\partial r^2} + \rho \frac{\partial}{\partial z} \left(\frac{1}{\rho} \frac{\partial p}{\partial z} \right) + k^2 p = 0. \quad (6)$$

The above equation can be equivalently written in the form of the following operator:

$$\left[\frac{\partial^2}{\partial r^2} + k_0^2 (1 + \mathcal{X}) \right] p = 0, \quad (7a)$$

$$\mathcal{X} = k_0^{-2} \left[\rho \frac{\partial}{\partial z} \left(\frac{1}{\rho} \frac{\partial}{\partial z} \right) + k^2 - k_0^2 \right], \quad (7b)$$

where $k_0 = 2\pi f/c_0$ and c_0 are the reference wavenumber and reference speed of sound, respectively. It is not difficult to see that Eq. (7a) can be decomposed into the following form, with separate terms corresponding to forward propagation and backward propagation:

$$\begin{aligned} & \left(\frac{\partial}{\partial r} - ik_0 \sqrt{1 + \mathcal{X}} \right) \left(\frac{\partial}{\partial r} + ik_0 \sqrt{1 + \mathcal{X}} \right) p \\ & + \left[\frac{\partial}{\partial r}, ik_0 \sqrt{1 + \mathcal{X}} \right] p = 0, \end{aligned} \quad (8)$$

where the square bracket denotes the commutator of the operators inside the bracket. In most cases, this commutator is calculated to be close to 0 and is negligible,

$$\left(\frac{\partial}{\partial r} - ik_0 \sqrt{1 + \mathcal{X}} \right) \left(\frac{\partial}{\partial r} + ik_0 \sqrt{1 + \mathcal{X}} \right) p = 0. \quad (9)$$

When we consider only forward propagation, the equation for one-way propagation becomes

$$\frac{\partial p}{\partial r} = ik_0 \sqrt{1 + \mathcal{X}} p. \quad (10)$$

In most cases, forward propagation dominates, while backward propagation is negligible. Thus, the original elliptical Helmholtz equation is reduced to a PE. When the solution method for ordinary differential equations is used, the above PE has a stepwise solution of the following form:

$$p(r + \Delta r, z) = \exp(i k_0 \Delta r \sqrt{1 + \mathcal{X}}) p(r, z). \quad (11)$$

It is difficult to directly solve Eq. (11) in a stepwise manner because the operator \mathcal{X} appears both under the square root and in the exponent. Here, we use the split-step Padé expansion technique proposed by Collins¹⁴ to address this exponential root operator. A Padé expansion of the exponential radical term yields a series of rational fractional multiplications:

$$p(r + \Delta r, z) = \exp(i k_0 \Delta r) \prod_{j=1}^n \frac{1 + a_j \mathcal{X}}{1 + b_j \mathcal{X}} p(r, z), \quad (12)$$

where n is the order of the Padé approximation and a_j and b_j are coefficients of the Padé approximation. Equation (12) can be solved after numerical discretization. For the initial field, either a self-starter or a normal-mode solution is used.

For a complete definite solution problem, the corresponding boundary and interface conditions should be accounted for during the numerical solution process. At the $(l-1)$ interfaces in the vertical direction, the sound pressure and the normal velocity of the particle should be continuous,

$$p_\ell(r, z)|_{z=h_\ell} = p_{\ell+1}(r, z)|_{z=h_\ell}, \quad (13a)$$

$$\frac{1}{\rho_\ell(r, z)} \frac{\partial p_\ell(r, z)}{\partial z} \Big|_{z=h_\ell} = \frac{1}{\rho_{\ell+1}(r, z)} \frac{\partial p_{\ell+1}(r, z)}{\partial z} \Big|_{z=h_\ell}. \quad (13b)$$

In addition, boundary conditions should be imposed on the sea surface and the seabed. Due to the significant difference in impedance between seawater and air, it is customary to set the sea surface as a pressure-release boundary, as shown in Eq. (14a),

$$p_1(r, 0) = 0, \quad (14a)$$

$$p_l(r, H) = 0, \quad (14b)$$

$$\frac{\partial p_l(r, z)}{\partial z} \Big|_{z=H} = 0. \quad (14c)$$

The seabed can be set as either a perfectly free or rigid boundary, corresponding to Eq. (14b) or Eq. (14c), respectively. In addition, in actual numerical simulations, the seabed is often set to an acoustic half-space. Traditionally, an artificial absorbing layer is usually used to truncate the acoustic half-space.^{20,50} In this paper, we use the perfectly matched layer (PML) technique to truncate the acoustic half-space.

B. PML technique for the acoustic half-space

In ocean acoustics, the seabed is often considered an acoustic half-space in which downward propagating sound waves meet the radiated boundary condition and attenuate to zero at infinity without creating any reflected waves on the seabed. In actual numerical simulations, the computational domain cannot be infinite, so this acoustic half-space needs to be truncated at an appropriate depth. This truncation involves creating a virtual interface, from which reflected waves will reach the area of interest above. To ensure that the reflected sound energy is low enough to be disregarded in the area of interest, it is typically necessary to truncate at a considerable depth and apply a high attenuation coefficient. This results in the creation of an artificial absorbing layer, which can be several wavelengths thick and

significantly slows computation, particularly for low-frequency sound sources. To overcome this limitation, we incorporate the PML technique into our algorithm. The PML technique was originally proposed by Berenger, who successfully used it for open-region electromagnetic scattering and radiation problems.⁵¹ Chew *et al.* introduced the PML technique into frequency-domain problems.⁵² Yevick *et al.* and Lu *et al.* attempted to introduce the PML technique into PE modeling and obtained good preliminary results. The following is a brief description of the PML technique used in our algorithm.^{53,54}

The core of the PML technique is the complex coordinate transformation. In Fig. 1, we define the following:

$$\tilde{z} = z + i \int_0^z \sigma(\tau) d\tau, \quad \begin{cases} \sigma(z) = 0, & z \in [0, H], \\ \sigma(z) > 0, & z \in [H, D]. \end{cases} \quad (15)$$

The truncated acoustic half-space is the PML, which is recorded as Layer ($l+1$) in order. By using \tilde{z} instead of z in the original governing equation and then solving the transformed new equation, the wave energy reflected from the PML can be attenuated to a very low level.

There are two main types of waves in the PML.

- For a downgoing ($z \rightarrow \infty$) plane wave, the solution is

$$\begin{aligned} p(r, z) &= p^{(d)} + p^{(u)} \\ &\simeq \exp[i(k_r r + k_z z)] + R \exp[i(k_r r - k_z z)], \end{aligned} \quad (16)$$

where $p^{(d)}$ and $p^{(u)}$ represent downward and upward waves, respectively; R is the reflection coefficient; and k_r and k_z are the horizontal and vertical wavenumbers, respectively, which satisfy $k_r^2 + k_z^2 = k_{l+1}^2$. The lower boundary of the PML is taken to be a pressure-release boundary $p_\ell(r, D) = 0$; thus, we obtain the following:

$$R = -\exp(2ik_z D) \exp\left(-2k_z \int_H^D \sigma(\tau) d\tau\right), \quad (17a)$$

$$|R| = \exp\left(-2k_z \int_H^D \sigma(\tau) d\tau\right). \quad (17b)$$

The larger σ is, the smaller the reflection coefficient. Moreover, for different k_z values, the reflection coefficient is different.

- In addition, waves that decay in the positive z direction should also be considered. Taking a range-independent waveguide as an example, the trapped modes are given in the following form:

$$\begin{aligned} p(r, z) &= p^{(d)} + p^{(u)} \\ &\simeq \exp[ik_r r - \gamma(z - H)] \\ &\quad + R \exp[ik_r r + \gamma(z - H)], \\ \gamma &= \sqrt{k_r^2 - k_{l+1}^2}. \end{aligned} \quad (18)$$

Similarly, by imposing the pressure-release condition at the lower boundary, we can obtain

$$R = -\exp[-2\gamma(D - H)] \exp\left(-2i\gamma \int_H^D \sigma(\tau) d\tau\right), \quad (19a)$$

$$|R| = \exp[-2\gamma(D - H)]. \quad (19b)$$

In this case, the reflection coefficient depends on γ and the thickness of the PML.

To make the PML as thin as possible (thereby reducing the demand for computing resources), we simply apply the following depth coordinate transformation:

$$\tilde{z} = z + \int_0^z [\gamma(\tau) + i\sigma(\tau)] d\tau. \quad (20)$$

Therefore,

$$\frac{\partial \tilde{z}}{\partial z} = g = 1 + \gamma(z) + i\sigma(z). \quad (21)$$

Substituting the above into Eq. (6), we obtain the following:

$$\frac{\partial^2 p}{\partial r^2} + \frac{\rho}{g} \frac{\partial}{\partial z} \left(\frac{1}{\rho g} \frac{\partial p}{\partial z} \right) + k^2 p = 0. \quad (22)$$

The depth operator now takes the following form:

$$\tilde{\mathcal{X}} = k_0^{-2} \left[\frac{\rho}{g} \frac{\partial}{\partial z} \left(\frac{1}{\rho g} \frac{\partial}{\partial z} \right) + k^2 - k_0^2 \right]. \quad (23)$$

In actual numerical simulations, the parameters of the PML can be considered to take the following forms:

$$\gamma(z) = \frac{100\tau(z)^3}{1 + \tau(z)^2}, \quad \sigma(z) = \frac{200\tau(z)^3}{1 + \tau(z)^2}, \quad \tau(z) = \frac{z - H}{D - H} \quad (24)$$

and the thickness of the PML can be set to only one wavelength, which will greatly shorten the run time.⁵⁴

III. SPECTRAL METHOD FOR THE WIDE-ANGLE PE MODEL

The basic principle of the spectral method is to use a set of orthogonal polynomials as the basis functions, project the function of interest into the subspace (also called the spectral space) formed by the orthogonal basis functions, and obtain the expanded coefficients (also called spectral coefficients). The operators and operational relations in differential equations can also be projected into the spectral space. Because of the particularity of the basis function, it is very convenient to solve differential equations in spectral space. After the spectral coefficients are obtained in the spectral space, the solution of the equation can be obtained by transforming it back into the physical space. The orthogonality of the basis functions and the smoothness of

the solution guarantee the exponential convergence of the spectral method.^{23–25}

A. Spectral method

In the spectral method, the principle of weighted residuals is adopted when discretizing a differential equation, that is, deriving the weak form, selecting the basis and weight functions, multiplying the residuals, and letting the weighted residuals equal to 0 to derive a series of algebraic equations. In classical spectral methods, the basis and weight functions are usually taken to be the same. In accordance with the type of basis functions chosen, spectral methods can be divided into many kinds. Here, we introduce a Chebyshev–Tau spectral method, in which the following Chebyshev polynomials are used as the basis functions:

$$\begin{aligned} T_0(t) &= 1; \quad T_1(t) = t; \quad T_2(t) = 2t^2 - 1, \\ T_{k+1}(t) &= 2tT_k(t) - T_{k-1}(t), \\ t \in [-1, 1], \quad k &= 2, 3, 4, \dots \end{aligned} \quad (25)$$

The Chebyshev polynomials $\{T_k(t)\}$ are defined on the interval $t \in [-1, 1]$, and their orthogonality is defined by the following formula:

$$\int_{-1}^1 \frac{T_k(t)T_l(t)}{\sqrt{1-t^2}} dt = \begin{cases} 0, & k \neq l, \\ \pi, & k = l = 0, \\ \frac{\pi}{2}, & k = l \geq 1. \end{cases} \quad (26)$$

A smooth function $u(t)$ on $t \in [-1, 1]$ can be expanded and approximated as follows:

$$u(t) = \sum_{k=0}^{\infty} \widehat{u}_k T_k(t) \simeq \sum_{k=0}^N \widehat{u}_k T_k(t), \quad (27)$$

where $\{\widehat{u}_k\}$ denotes the spectral coefficients of $u(t)$ and N is the order of spectral truncation. With increasing N , the error of this approximation will exponentially decrease. According to the orthogonality of the Chebyshev polynomials, the spectral coefficients $\{\widehat{u}_k\}$ in the above formula can be obtained as follows:

$$\widehat{u}_k = \frac{2}{\pi c_k} \int_{-1}^1 \frac{u(t)T_k(t)}{\sqrt{1-t^2}} dt, \quad c_k = \begin{cases} 2, & k = 0, \\ 1, & k > 0. \end{cases} \quad (28)$$

With the above two equations, the back-and-forth mapping of a function between the physical space and the spectral space can be easily achieved. The integration in Eq. (28) is usually evaluated through numerical schemes. For improved accuracy, a special Gaussian quadrature, the Gauss–Chebyshev–Lobatto (GCL) quadrature, is generally used. The nodes and weights of the GCL quadrature are given below,

$$t_j = \cos\left(\frac{j\pi}{N}\right), \quad j = 0, 1, 2, \dots, N,$$

$$\widehat{u}_k \simeq \frac{1}{d_k} \sum_{j=0}^N u(t_j) T_k(t_j) w_j, \quad k = 0, 1, 2, \dots, N,$$

$$w_j = \begin{cases} \frac{\pi}{2N}, & j = 0, N, \\ \frac{\pi}{N} & \text{otherwise,} \end{cases} \quad d_k = \begin{cases} \pi, & k = 0, N, \\ \frac{\pi}{2} & \text{otherwise.} \end{cases} \quad (29)$$

The derivative of the function $u(t)$ can be similarly expanded as follows:

$$u'(t) = \sum_{k=0}^{\infty} \widehat{u}'_k T_k(t) = \left(\sum_{k=0}^{\infty} \widehat{u}_k T_k(t) \right)' = \sum_{k=0}^{\infty} \widehat{u}_k T'_k(t). \quad (30)$$

According to the relationship between the Chebyshev polynomials and their derivatives, it is easy to obtain the following relationship:²⁶

$$\widehat{u}'_k \simeq \frac{2}{c_k} \sum_{\substack{m=k+1, \\ m+k=\text{odd}}}^N m \widehat{u}_m, \quad (31a)$$

$$\widehat{\mathbf{u}}' \simeq \mathbf{D}_N \widehat{\mathbf{u}}. \quad (31b)$$

Equation (31b) is the matrix-vector form of the derivative relationship, \mathbf{D}_N is a square matrix of order $(N+1)$, and $\widehat{\mathbf{u}}$ is the column vector composed of $\{\widehat{u}_k\}_{k=0}^N$. The spectral coefficients of the product of two functions have the following relationship:²⁴

$$\widehat{v}\widehat{u}_k \approx \frac{1}{2} \sum_{m+n=k}^N \widehat{u}_m \widehat{v}_n + \frac{1}{2} \sum_{|m-n|=k}^N \widehat{u}_m \widehat{v}_n, \quad (32a)$$

$$\widehat{\mathbf{v}}\widehat{\mathbf{u}} \simeq \mathbf{C}_v \widehat{\mathbf{u}}. \quad (32b)$$

Other relationships not used in this article will not be described here.

B. Numerical discretization

The key to solving the wide-angle PE model is the stepwise advancement in Eq. (12), and the key to this advancement is the discretization of the depth operator \mathcal{X} . Next, we attempt to discretize the wide-angle PE model using the Chebyshev spectral method. Before the spectral transformation is performed, the solution domain $[z_1, z_2]$ is first scaled to $t \in [-1, 1]$,

$$t = \frac{2z}{z_2 - z_1} - \frac{z_2 + z_1}{z_2 - z_1}, \quad \frac{dt}{dz} = \frac{2}{z_2 - z_1}.$$

Therefore, the depth operator \mathcal{X} and Eq. (12) become

$$\mathcal{X} = k_0^{-2} \left[\frac{4}{\Delta z^2} \rho(t) \frac{\partial}{\partial t} \left(\frac{1}{\rho(t)} \frac{\partial}{\partial t} \right) + k^2 - k_0^2 \right], \quad (33a)$$

$$p(r + \Delta r, t) = \exp(i k_0 \Delta r) \prod_{j=1}^n \frac{1 + a_j \mathcal{X}}{1 + b_j \mathcal{X}} p(r, t), \quad (33b)$$

where Δz is the thickness of the waveguide. According to the relationships in Eqs. (31) and (32), the discrete forms of the operator \mathcal{X} and Eq. (12) in the Chebyshev spectral space are

$$\mathbf{X} = k_0^{-2} \left(\frac{4}{\Delta z^2} \mathbf{C}_\rho \mathbf{D}_N \mathbf{C}_{1/\rho} \mathbf{D}_N + \mathbf{C}_{k^2} - k_0^2 \mathbf{I}_N \right), \quad (34a)$$

$$\hat{\mathbf{p}}(r + \Delta r, t) = \exp(i k_0 \Delta r) \prod_{j=1}^n \frac{\mathbf{I}_N + a_j \mathbf{X}}{\mathbf{I}_N + b_j \mathbf{X}} \hat{\mathbf{p}}(r, t), \quad (34b)$$

where \mathbf{I}_N is the identity matrix of order $(N + 1)$. The weak form of the differential equation and the process of weighted residual minimization involved in the spectral discretization of Eq. (33) can be found in Sec. 3.2 of Ref. 47. Equation (34b) is solved in the following way:

$$\begin{aligned} & \prod_{j=1}^n (\mathbf{I}_N + b_j \mathbf{X}) \hat{\mathbf{p}}(r + \Delta r, t) \\ &= \exp(i k_0 \Delta r) \prod_{j=1}^n (\mathbf{I}_N + a_j \mathbf{X}) \hat{\mathbf{p}}(r, t) \end{aligned} \quad (35)$$

and each iteration step requires solving n linear equations of order $(N + 1)$. The matrices are defined as follows:

$$\mathbf{L}_j = \mathbf{I}_N + b_j \mathbf{X}, \quad \mathbf{R}_j = \mathbf{I}_N + a_j \mathbf{X}.$$

We let the propagator matrix \mathbf{T} be expressed as follows:

$$\mathbf{T} = \prod_{j=1}^n (\mathbf{L}_j^{-1} \mathbf{R}_j).$$

Thus, Eq. (35) can be written as

$$\hat{\mathbf{p}}(r + \Delta r, t) = \exp(i k_0 \Delta r) \mathbf{T} \hat{\mathbf{p}}(r, t). \quad (36)$$

In Fig. 1, there are discontinuities in the acoustic properties of the media in the vertical direction; that is, the waveguide is composed of multiple layers of media with different properties. Due to the requirements of spectral methods regarding the smoothness of functions, a set of Chebyshev bases cannot accurately approximate the piecewise continuous sound speed, density, and attenuation. A natural idea is to adopt the strategy of domain decomposition,⁵⁵ that is, in different layers, different numbers of Chebyshev bases are used for expansion and discretization (the number of bases, i.e., the order of spectral truncation, depends on the thickness of the medium and the complexity of the acoustic parameters). Similar to Eq. (34), the depth operator and governing equation of the ℓ -th layer can be discretized as follows:

$$\mathbf{X}_\ell = k_0^{-2} \left[\frac{4}{(h_\ell - h_{\ell-1})^2} \mathbf{C}_{\rho_\ell} \mathbf{D}_{N_\ell} \mathbf{C}_{1/\rho_\ell} \mathbf{D}_{N_\ell} + \mathbf{C}_{k_\ell^2} - k_0^2 \mathbf{I}_{N_\ell} \right], \quad (37a)$$

$$\begin{aligned} & \prod_{j=1}^n (\mathbf{I}_{N_\ell} + b_j \mathbf{X}_\ell) \hat{\mathbf{p}}_\ell(r + \Delta r, t) \\ &= \exp(i k_0 \Delta r) \prod_{j=1}^n (\mathbf{I}_{N_\ell} + a_j \mathbf{X}_\ell) \hat{\mathbf{p}}_\ell(r, t). \end{aligned} \quad (37b)$$

Since all layers need to step forward together, the \mathbf{X}_ℓ operators and Eq. (37b) for all l layers should be assembled into a global form as follows:

$$\mathbf{X} = \begin{bmatrix} \mathbf{X}_1 & \mathbf{0} & \mathbf{0} & \mathbf{0} \\ \mathbf{0} & \mathbf{X}_2 & \mathbf{0} & \mathbf{0} \\ \mathbf{0} & \mathbf{0} & \ddots & \mathbf{0} \\ \mathbf{0} & \mathbf{0} & \mathbf{0} & \mathbf{X}_l \end{bmatrix}, \quad \hat{\mathbf{p}} = \begin{bmatrix} \hat{\mathbf{p}}_1 \\ \hat{\mathbf{p}}_2 \\ \vdots \\ \hat{\mathbf{p}}_l \end{bmatrix}. \quad (38)$$

The global matrix \mathbf{X} is a block diagonal square matrix of order $\sum_{\ell=1}^l (N_\ell + 1)$. Next, we discuss how boundary conditions and interface conditions are imposed. Among spectral methods, the Galerkin-type spectral method first seeks basis functions satisfying the boundary conditions to ensure that the discretized linear equations will naturally satisfy the boundary conditions. However, this approach lacks flexibility when dealing with even slightly complex boundary conditions, as it may be difficult to construct an appropriate basis set. In this paper, we utilize a Chebyshev Tau-type spectral method instead. This method eliminates the need for preconstructed basis functions that satisfy the boundary conditions; instead, those conditions are transformed into the spectral space, and the linear equations derived from the projection of both the boundary conditions and the discretized governing equation are solved simultaneously. For convenience of description, we define the following row vectors:

$$\begin{aligned} \mathbf{s}_\ell &= [s_0, s_1, s_2, \dots, s_{N_\ell}], s_i = T_i(-1) = (-1)^i, \\ \mathbf{q}_\ell &= [q_0, q_1, q_2, \dots, q_{N_\ell}], q_i = T_i(+1) = 1. \end{aligned}$$

The boundary and interface conditions in Eqs. (13) and (14) are spectrally discretized as follows:

$$\mathbf{s}_\ell \mathbf{p}_\ell - \mathbf{q}_{\ell+1} \mathbf{p}_{\ell+1} = \mathbf{0}, \quad (39a)$$

$$\begin{aligned} & \frac{1}{(h_\ell - h_{\ell-1}) \rho_\ell(r, h_\ell)} \mathbf{s}_\ell \mathbf{D}_{N_\ell} \mathbf{p}_\ell \\ & - \frac{1}{(h_{\ell+1} - h_\ell) \rho_{\ell+1}(r, h_\ell)} \mathbf{q}_{\ell+1} \mathbf{D}_{N_{\ell+1}} \mathbf{p}_{\ell+1} = \mathbf{0}, \end{aligned} \quad (39b)$$

$$\mathbf{q}_1 \mathbf{p}_1 = \mathbf{0}, \quad (39c)$$

$$\mathbf{s}_l \mathbf{p}_l = \mathbf{0}, \quad (39d)$$

$$\mathbf{s}_l \mathbf{D}_{N_l} \mathbf{p}_l = \mathbf{0}. \quad (39e)$$

As shown in Fig. 1, there are $(l - 1)$ interfaces in l layers of media, leading to $2(l - 1)$ sets of interface conditions. Furthermore, both the sea surface and seabed have boundary conditions, for a total of $2l$ sets of conditions.

To ensure that the system of linear equations remains well defined after the incorporation of boundary/interface conditions, some equations will need to be discarded. Based on the convergence of the spectral approximation, we replace the last two rows of each subblock in the matrix \mathbf{X} (rows N_ℓ and $N_{\ell+1}$) with boundary or interface conditions. This is equivalent to using the last two rows of the spectral matrix \mathbf{X}_ℓ for the ℓ -th layer of media to impose boundary or interface conditions, which reduces the accuracy of the spectral approximation from $(N_\ell + 1)$ to $(N_\ell - 1)$. However, this two-order reduction in accuracy can be simply compensated by increasing N_ℓ .

The method for assembling the global matrix described above is suitable when the lower boundary of the waveguide is either perfectly free or rigid. However, if the lower boundary is an acoustic half-space, it is truncated to a PML at a depth of one wavelength. Although the PML is treated similarly to the ordinary layers in terms of spectral discretization, the discrete form of the depth operator is different,

$$\begin{aligned} \mathbf{X}_{l+1} = k_0^{-2} & \left[\frac{4}{(D-H)^2} \mathbf{C}_{\rho_{l+1}/g} \mathbf{D}_{N_{l+1}} \mathbf{C}_{1/(g\rho_{l+1})} \mathbf{D}_{N_{l+1}} \right. \\ & \left. + \mathbf{C}_{k_{l+1}^2} - k_0^2 \mathbf{I}_{N_{l+1}} \right]. \end{aligned} \quad (40)$$

The spectral truncation order N_{l+1} in the PML can be taken to be a small value, for example, 5–10.

Lateral inhomogeneity produces changes in only the acoustic parameters, and without topographic relief, energy

in the vertical direction is naturally conserved. When a new acoustic parameter is encountered during a lateral step, all that is necessary to continue the stepping process is to update the depth matrix \mathbf{X} . Conversely, during long segments in which the acoustic parameters remain homogeneous, each iteration step requires only a matrix multiplication operation as per Eq. (36).

IV. NUMERICAL EXPERIMENTS AND VALIDATION

Based on the spectral algorithm proposed in this paper, we developed a numerical software package called SMPE. Next, we assess the reliability, applicability, and performance of the proposed algorithm by comparing its simulation results with those obtained using existing, mature software.

A. Analytical example: Pseudolinear-speed waveguides

A pseudolinear-speed waveguide is a range-independent waveguide in which the sound speed profile has the following form:⁵⁶

$$c(z) = \sqrt{\frac{1}{az + b}}. \quad (41)$$

In this example, we consider a sea depth of $H = 100$ m, $a = 5.94 \times 10^{-10} \text{ s}^2/\text{m}^3$, and $b = 4.16 \times 10^{-7} \text{ s}^2/\text{m}^3$; the

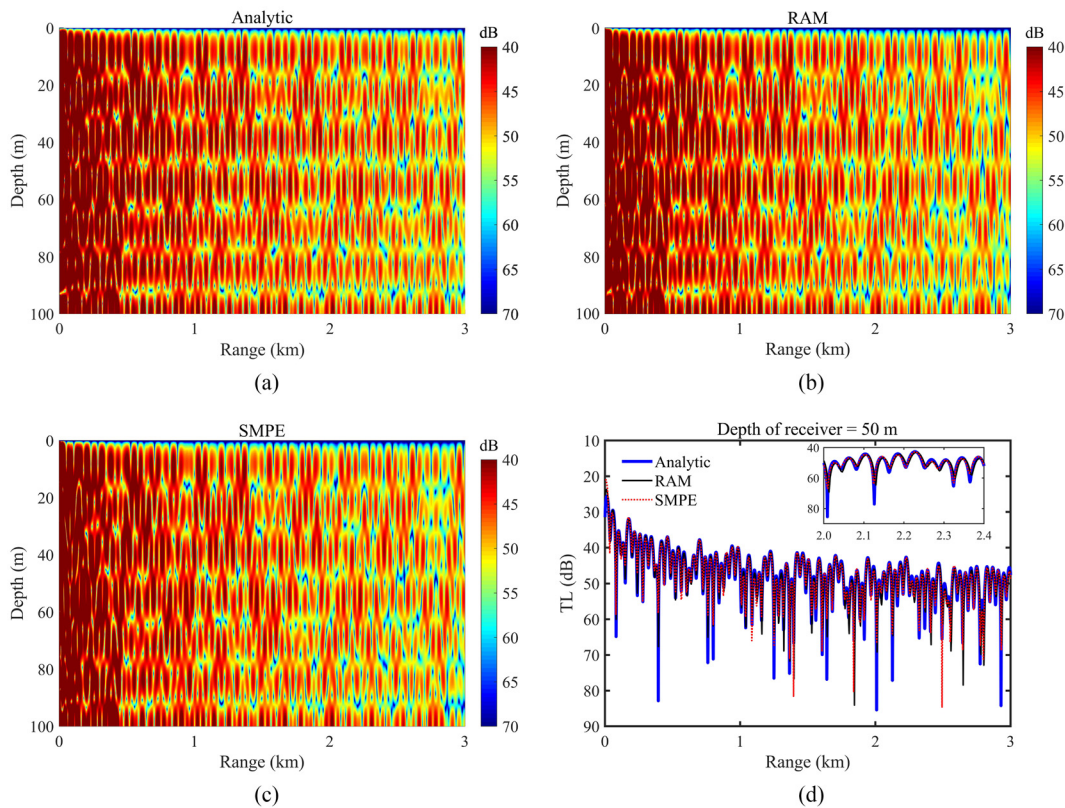


FIG. 2. (Color online) Sound fields of a pseudolinear-speed waveguide with a perfectly rigid bottom as calculated using the analytical solution (a), RAM (b), and SMPE (c) and the TL vs range curves at a depth of $z = 50$ m (d).

sound source is located at a depth of $z_s = 36$ m, the sound frequency is $f = 50$ Hz, and the density of the seawater is set to $\rho = 1 \text{ g/cm}^3$. n is set to 10 in both SMPE and RAM. Pseudolinear-speed waveguides with both a pressure-release and a perfectly rigid bottom have analytical solutions; accordingly, the error can be visually displayed to analyze the computational accuracy of the proposed algorithm.

Figure 2 depicts the sound fields of a pseudolinear-speed waveguide with a rigid seabed as computed using the analytical solution, RAM, and SMPE. The pseudocolor diagrams show that both SMPE and RAM exhibit no significant differences from the analytical solution. An in-depth comparison of the TL curves at a depth of 50 m reveals that SMPE closely aligns with the analytical solution, while RAM experiences minor phase errors, particularly in the peaks.

Figures 3(a)–3(c) show the corresponding sound fields of a pseudolinear-speed waveguide with a pressure-release seabed. Significantly, the three results are almost completely identical. The TL curves at a depth of $z = 50$ m in Fig. 3(d) overlap almost entirely, which illustrates that the results of both RAM and SMPE are highly accurate except for the range very close to the sound source. The number of grid points used in RAM is 400, while the truncation order in SMPE is only 30.

To further compare the accuracy of SMPE in this experiment, Fig. 4(a) shows the TL curves at a depth of $z = 50$ m calculated by RAM and SMPE, and Fig. 4(b) shows the

errors corresponding to the curves in Fig. 4(a). A significant trend is that as the number of grid points increases from 50 to 500, the RAM results gradually approach the analytical solution, and the error gradually decreases toward zero. When the number of grid points used in RAM is 50, 100, or 200, the error of the simulation results is too large to be satisfactory. Even with 500 grid points, RAM is still not as accurate as SMPE. As seen in Fig. 4(b), when the number of grid points in RAM is 400 or 500, the error is already relatively small but still significantly higher than the error of SMPE. Therefore, we can tentatively conclude that compared with RAM, which requires a considerable number of grid points, SMPE can achieve higher accuracy with a relatively small truncation order.

To obtain a more convincing conclusion, we combine the whole sound field to test the accuracy of SMPE. The average of the absolute errors between the numerical and analytical sound pressure fields is used to compare the accuracy of the programs. Figure 5 depicts the variation in the errors of RAM and SMPE with increasing N , where N represents the number of discrete points in RAM or the truncation order in SMPE. Overall, for both SMPE and RAM, the global average error first decreases and then stabilizes at a certain value. As the number of grid points increases from 25 to 400, the error of RAM decreases roughly linearly, and at $400 < N < 1000$, the error stabilizes at approximately 0.34 dB. Once N exceeds 1000, increasing N increases the error. As the spectral truncation order is increased

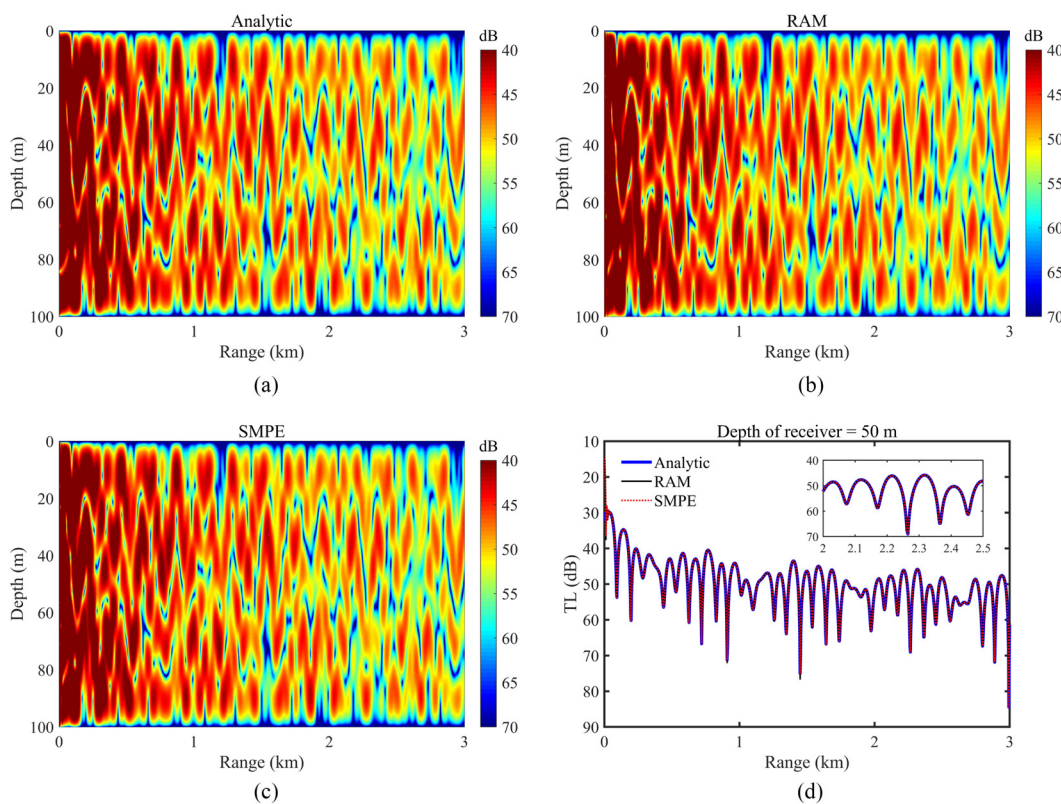


FIG. 3. (Color online) Sound fields of a pseudolinear-speed waveguide with a pressure-free bottom as calculated using the analytical solution (a), RAM (b), and SMPE (c) and the TL vs range curves at a depth of $z = 50$ m (d).

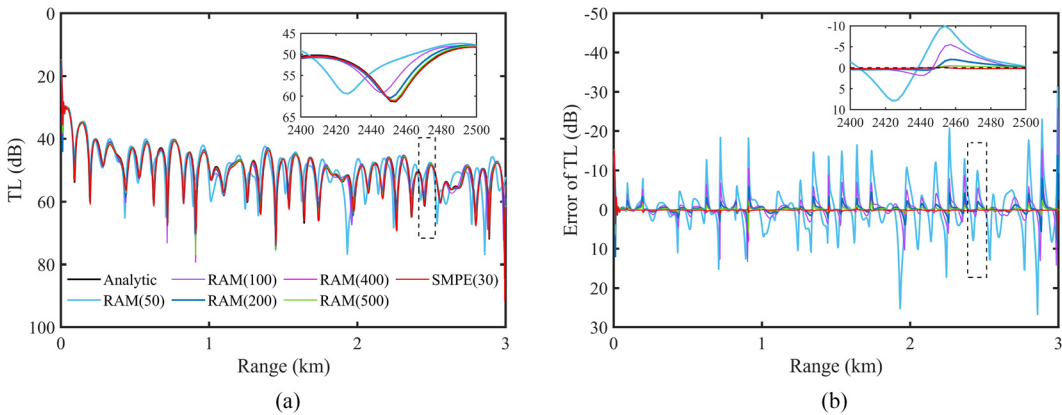


FIG. 4. (Color online) TL vs range curves (a) and errors with respect to the analytical solution (b) calculated using RAM and SMPE at a depth of $z = 50$ m. The number in brackets after “RAM” in the legend corresponds to the number of grid points taken in the vertical direction, and the “30” in brackets after “SMPE” indicates the truncation order.

from 10 to 30, the error of SMPE quickly converges to 0.35 dB. Then, this error continues to decrease and tends to become stable at truncation orders above 100. The rate of error convergence matches an exponential function very well, which verifies the conclusion from mathematics that the error of spectral methods converges exponentially.²⁴ In this particular example, SMPE needs a spectral truncation order of only 30 to achieve the minimum error that RAM can achieve. Moreover, SMPE’s minimum error is merely 0.038 dB, which is an accuracy that the RAM program cannot reach, regardless of how many discrete points are utilized. Compared to the analytical solution, both discrete methods produce accurate results. Furthermore, in this example, the accuracy and convergence rate of the spectrally discretized SMPE program surpass those of RAM, which employs the finite difference method. These findings underscore the superiority of the new algorithm.

B. Plane-parallel waveguide

Next, we consider a plane-parallel waveguide, in which the sound speed is dependent on the horizontal range and depth. Figure 6(a) intuitively displays the sound speed of the plane-parallel waveguide. In this example, the depth is taken to be $H = 500$ m, and the sound speed $c(r, z)$ is expressed as follows:⁵⁷

$$\frac{c_0^2}{c^2(r, z)} = 1 + \frac{\pi^2 f_1^2}{H^2} \exp\left(-\frac{2\pi r}{H}\right) + \frac{4\pi^2 f_2^2}{H^2} \exp\left(-\frac{4\pi r}{H}\right) - \frac{2\pi f_1}{H} \left[1 - \frac{2\pi^2 f_2^2}{H} \exp\left(-\frac{2\pi r}{H}\right)\right] \times \cos\left(\frac{\pi z}{H}\right) \exp\left(-\frac{\pi r}{H}\right) - \frac{4\pi f_2}{H} \cos\left(\frac{2\pi z}{H}\right) \exp\left(-\frac{2\pi r}{H}\right), \quad (42)$$

where $c_0 = 1500$ m/s, $f_1/H = 0.032$, and $f_2/H = 0.016$. In this example, the source frequency is $f = 25$ Hz, the sound source is located at a depth of $z_s = 250$ m, and the density of the seawater is taken to be $\rho = 1$ g/cm³. n is taken to be 8 in both SMPE and RAM; the truncation order in SMPE is 90, and the number of grid points in RAM is 1000. Figure 7 shows the sound fields and TL curves of the plane-parallel waveguide, which has a pressure-release bottom, as calculated using COUPLE, RAM, and SMPE. COUPLE is a program based on coupled modes, and its results can usually be used as benchmarks in ocean acoustics.⁵⁰ The sound field results from the three programs display a high degree of consistency, indicating that SMPE can also produce a reliable acoustic field in a laterally inhomogeneous waveguide. Similar conclusions can be drawn for a plane-parallel

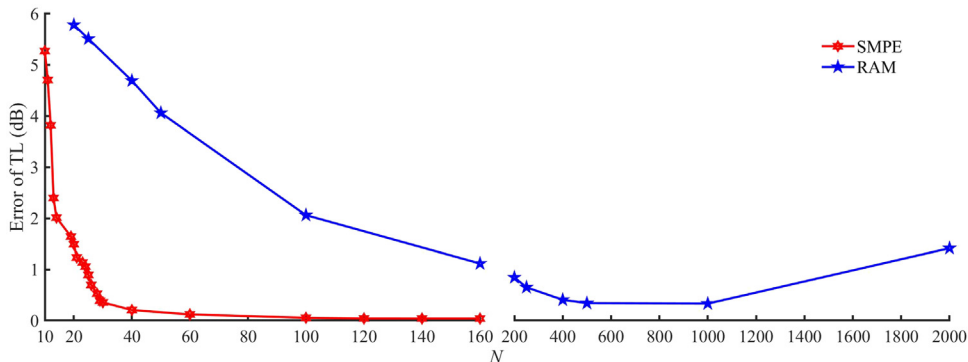


FIG. 5. (Color online) Variation in the errors of RAM and SMPE with increasing N .

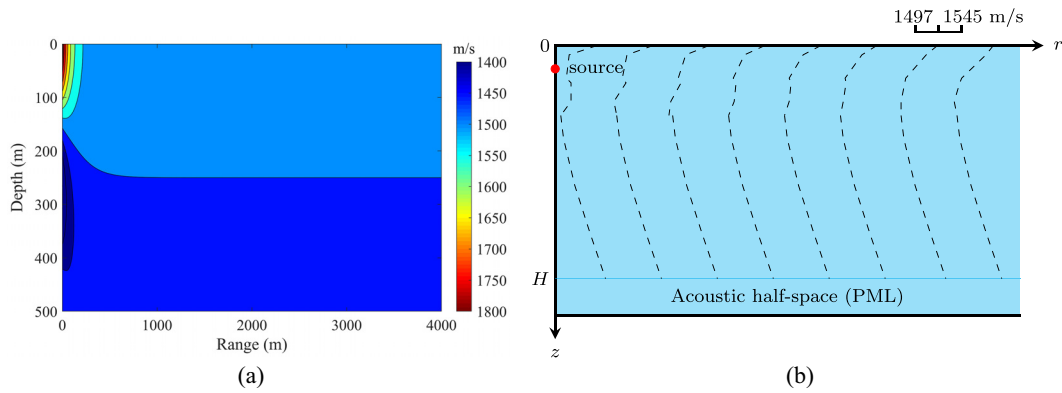


FIG. 6. (Color online) Sound speeds in the plane-parallel waveguide (a) and warm-core eddy (b). The sound speed profiles in (b) vary at ranges of 0, 12.5, 25, 37.5, 50, 75, and 100 km.

waveguide with a rigid bottom, for which numerical simulations reaffirm that the SMPE results closely align with the benchmark, regardless of whether the TL is computed across the complete field or at a particular receiving depth—this point requires no further elaboration.

C. Warm-core eddy

A variety of mesoscale movements can occur in the ocean that perturb sound propagation in media by changing the acoustic parameters of the media. For example, the presence of eddies can have a great impact on the distribution of

sound energy in the ocean. In this case, we consider a warm-core eddy with seven sound speed profiles, as shown in Fig. 6(b) (dashed lines). The depth is $H = 5000$ m, the source frequency is $f = 50$ Hz, the sound source is located at a depth of $z_s = 300$ m, the density of the water is set to $\rho = 1 \text{ g/cm}^3$, and the bottom is an acoustic half-space (the sound speed is continuous with the first profile, with a density of 1 g/cm^3 and no attenuation). n is taken to be 4 in both SMPE and RAM. To truncate the acoustic half-space, an artificial absorbing layer with a thickness of 5000 m is set in RAM, and the attenuation within this layer is increased from 0 to 10. The truncation order in SMPE is 500, while the number

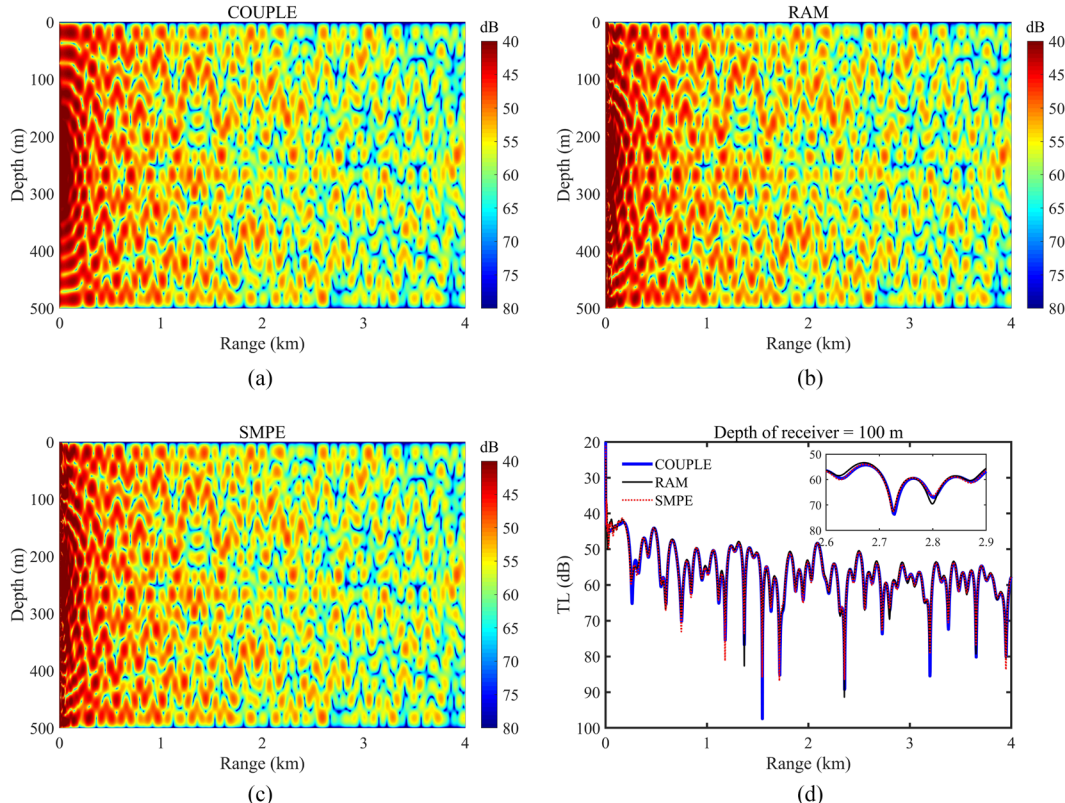


FIG. 7. (Color online) Sound fields of a plane-parallel waveguide with a pressure-release bottom as calculated using COUPLE (a), RAM (b), and SMPE (c) and the TL vs range curves at a depth of $z = 100$ m (d).

of grid points used in RAM is 10 000. Figure 8 shows plots of the sound fields throughout the warm-core eddy as calculated using KRAKEN,⁵⁸ SPEC, RAM, and SMPE. SPEC is a two-way coupled-mode model based on a spectral method.^{36,37} When near-field leaky modes are ignored, the SPEC results can be regarded as the benchmark solution. The KRAKEN results in the solid wireframe regions are obviously different from those of the other three models because the range dependence in KRAKEN is treated by means of one-way coupled-mode theory. In the far field, the sound fields calculated via SPEC, RAM, and SMPE are in good agreement, which further demonstrates the ability of SMPE to simulate laterally inhomogeneous waveguides with acoustic half-spaces.

V. DISCUSSION

A. Discussion of the parameters of SMPE

1. Number of layers and spectral truncation orders

From the perspective of algorithm completeness and model robustness, treating a continuous medium as a discontinuous medium should still yield correct results. Taking the warm-core eddy experiment in Sec. IV C as an example, we explore the characteristics of the solution when a continuous medium is layered.

Figure 9 shows the acoustic fields simulated by SMPE under different layering conditions in this experiment. When

the medium is layered, the spectral truncation orders corresponding to the single-layer media are distributed proportionally to the thickness of each layer. The spectral truncation order in Fig. 9(a) is 500. For the top and bottom layers in Fig. 9(b), their spectral truncation orders are 150 and 350, respectively. For the three layers in Fig. 9(c), their respective spectral truncation orders are 150, 150, and 200 from top to bottom. Similarly, for the four layers in Fig. 9(d), their respective spectral truncation orders are 150, 150, 100 and 100. It can be clearly seen from Fig. 9 that for continuous media, regardless of where the layering is done or how many layers there are, SMPE can obtain correct results.

Note that the above analysis was conducted under the premise that the total truncation order is sufficiently high. In fact, it cannot be guaranteed that multiple layers can still yield accurate results under more general conditions. Figure 10 displays the sound fields simulated by SMPE when the truncation orders are half of those in Fig. 9. The distortion in the near field in Fig. 10(a) indicates that the spectral approximation of order $N=250$ is slightly insufficient in this simulation. As the number of layers increases, the range of the near-field distortion also increases, indicating that increasing the number of layers while keeping the total spectral truncation order unchanged will decrease the accuracy of the simulation.

This is theoretically in line with the mathematical principles of the spectral algorithm proposed in this paper. The spectrally discretized matrix of a single-layer medium is

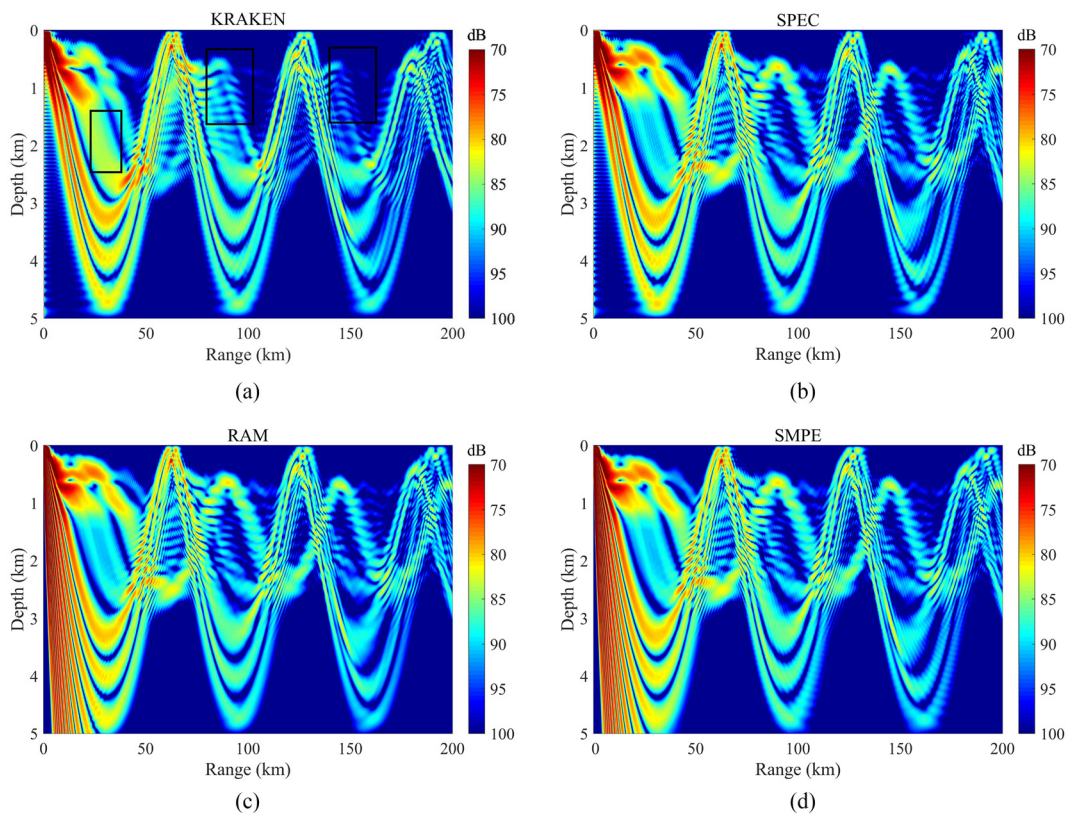


FIG. 8. (Color online) Sound fields in a warm-core eddy region with an acoustic half-space as calculated using KRAKEN (a), SPEC (b), RAM (c), and SMPE (d).

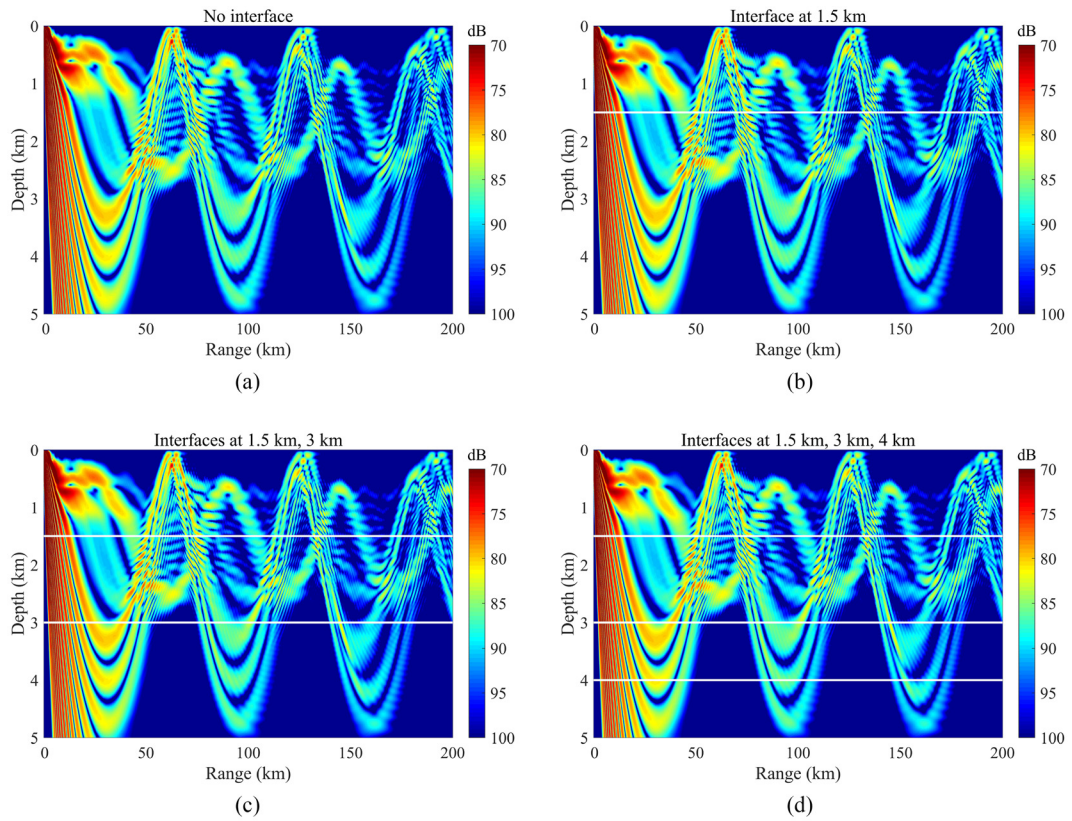


FIG. 9. (Color online) Numerical sound fields in the warm-core eddy experiment as calculated by SMPE under different vertical layering schemes (solid white lines indicate the positions of the virtual interfaces).

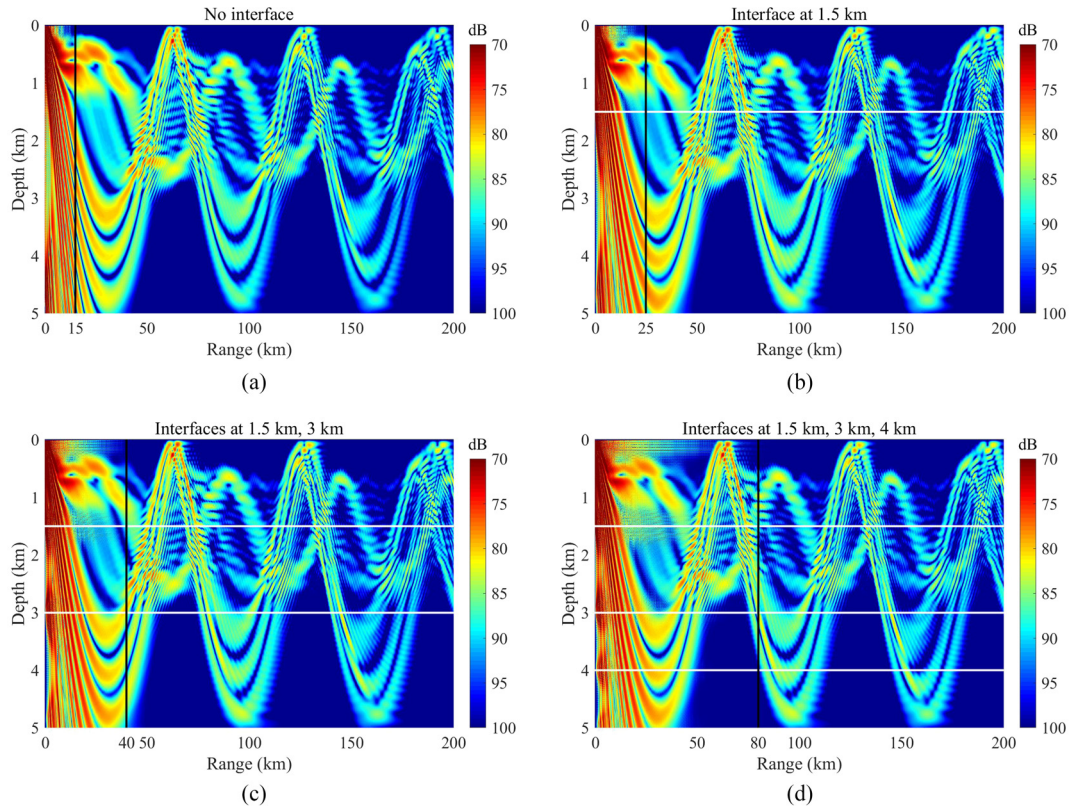


FIG. 10. (Color online) Sound fields simulated by SMPE when the spectral truncation order is halved relative to Fig. 9 (solid black lines mark where the distortion of the sound field disappears).

large and dense, while that of a multilayer medium is a block diagonal matrix composed of multiple small dense matrices, as shown in Eq. (38). The increase in sparsity leads to a decrease in computational cost but also implies a loss of accuracy. Therefore, for simulations of multilayer media, the truncation order should be carefully selected based on the thickness of each layer and the complexity of the acoustic parameters to ensure the reliability of the simulation results.

2. Order of Padé approximation

In the numerical examples of Sec. VA 1, the orders in the Padé approximation series for both RAM and SMPE were set to the same value. The purpose was to control other variables in order to investigate the impact of a single factor, i.e., the numerical discretization method, on the simulation accuracy. However, the sensitivity of the accuracy of SMPE to the order of Padé approximation should be further analyzed and discussed.

We take the pseudolinear-speed waveguide with a free seabed in Sec. IV A as an example to study the trends of the simulation errors of SMPE and RAM with variations in the range step size under different orders of Padé approximation. Figure 11 shows the variation trends of the acoustic field errors of SMPE and RAM with respect to Δr for four different orders of Padé approximation. The number of grid points in the vertical direction in RAM is 200, the spectral

truncation order in SMPE is 30, and other parameters remain consistent. It can be seen from Fig. 11(a) that when the order of Padé approximation is set to 4, the simulation errors of both SMPE and RAM exhibit the same trend as the step size changes, with an initial decrease followed by an increase, and the numerical differences are also very minor. From Figs. 11(b)–11(d), the trend of error variation with the step size remains unchanged for both models, but as n increases, the tolerable range step size also increases. In terms of accuracy, with increasing n , SMPE has a certain advantage over RAM. In addition, it can be seen that the minimum allowed range step size for SMPE is larger than that for RAM because when the range step size is too small, SMPE's error is larger than that of RAM.

B. Discussion of the performance of SMPE

In addition to correctness, the performance of a new model is the most important concern in actual simulation. To visually and quantitatively demonstrate the performance of the algorithm proposed in this article, Table I lists the run times of SMPE and RAM for the numerical examples in Sec. IV. The numerical examples were run on the same computer (HUAWEI Matebook Xpro 2017), which is equipped with an Intel-i7 8550 U processor and 16 GB of memory. Because SMPE is written in MATLAB, for fair comparison, the RAM implementation used in these tests was the MATLAB version implemented by Dzieciuch and

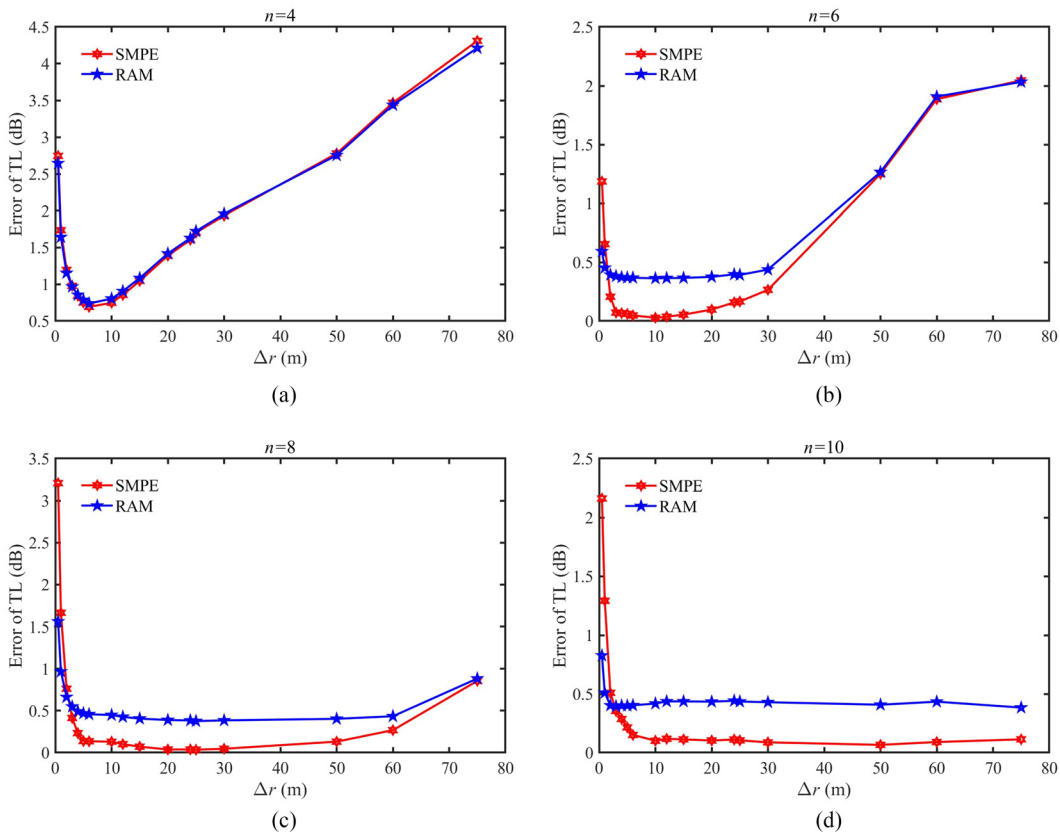


FIG. 11. (Color online) Variation trends of the acoustic field errors as calculated by the two models with the range step size under different orders of Padé approximation.

TABLE I. Run times for numerical experiments (unit: s).

Experiment	Software	
	RAM	SMPE
Pseudolinear (rigid bottom)	4.940	0.059
Pseudolinear (free bottom)	1.357	0.057
Plane-parallel (free bottom)	12.240	11.307
Plane-parallel (rigid bottom)	18.928	13.254
Warm-core eddy	22.019	6.472

published in OALIB.⁵⁹ To provide a stable measure of performance, the run times listed in the table are each the average value over ten tests.

The pseudolinear-speed waveguides serve as simple range-independent examples, in which SMPE exhibits an advantage of more than an order of magnitude in computational efficiency over RAM. For this kind of shallow-water and range-independent waveguide, the iterative process in SMPE does not require frequent updates of \mathbf{X} but only calls for matrix multiplication operations [see Eq. (36)], which greatly reduces the amount of calculation. In addition, the spectral approximation requires only a relatively small order, which also leads to smaller and easier-to-solve matrices. The plane-parallel waveguides represent examples that are horizontally inhomogeneous, requiring updates to \mathbf{X} in each iteration step for both models. Nevertheless, SMPE shows a speed advantage thanks to the smaller matrices discretized via the Chebyshev spectral method. The main feature of the warm-core eddy waveguide is that it contains a homogeneous acoustic half-space. For this example, the table shows that SMPE is more than three times faster than RAM. On the one hand, the matrices formed via spectral discretization are smaller. Another important contributing factor is that SMPE uses the PML technique to simulate the acoustic half-space. The PML perfectly absorbs downward waves, and this layer is also very thin, which greatly improves the computational efficiency of SMPE. Notably, RAM uses a high-density artificial absorbing layer to simulate the rigid seabed, whereas SMPE avoids this by imposing a lower boundary [Eq. (14c)], making it faster than RAM.

C. Discussion of the range dependence of terrain

The above numerical experiments validate the accuracy of SMPE in the simulation of laterally inhomogeneous acoustic waveguides. A natural question is why SMPE is inadequate in addressing the range dependence of topographic relief. Typically, topographic relief is approximated by flat steps, as illustrated in Fig. 12.⁵⁰ This approximation suffices if the step width is suitably narrow.

The widely used “stair-step” approach in simulating ocean acoustics is not compatible with SMPE due to the varying terrain undulation. Specifically, the layer thickness changes before and after each stepwise iteration, resulting in a change in the solution domain for the spectral method. In the Chebyshev spectral transformation, the function values

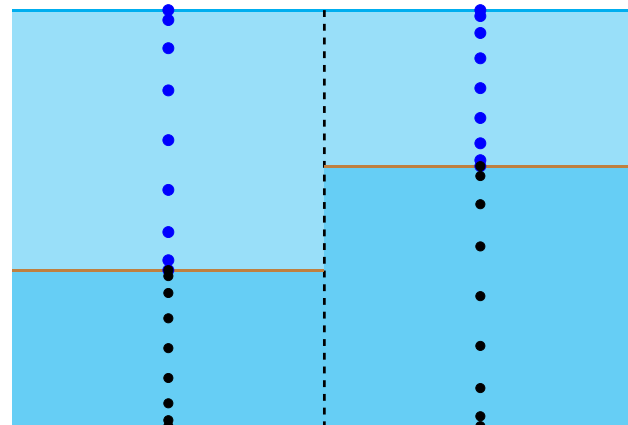


FIG. 12. (Color online) GCL nodes (blue and black dots) for handling a sloping interface. The slope is approximated by a series of stair steps with rises and runs. The two horizontal brown lines are runs. The black dashed line is a vertical interface between two range-independent segments, which includes a rise.

from the GCL nodes in the defined domain are taken to fit the complete function in the physical space, and this function is then mapped to the spectral space. The GCL nodes form a set of nonequidistant nodes that are sparse in the center and dense at both ends. These nodes are generated by scaling the extrema of the Chebyshev polynomial $T_N(t)$ on $t \in [-1, 1]$ to the solution domain.²⁴ However, the variable nature of the solution domain caused by terrain fluctuation renders the new spectral coefficients invalid after the original coefficients have stepped to the next range. In fact, even if the new spectral coefficients are inverse-transformed back into the physical space, an incorrect solution will be produced. From the perspective of numerical quadrature, the fundamental requirement for correct calculation in Eq. (28) is exact matching of the nodes and the integrand interval.

VI. REMARKS AND SUMMARY

Based on the above analysis and discussion, we can observe that the algorithm proposed in this article possesses the following distinctive characteristics.

A. Remarks

- (1) This paper presents a spectral algorithm for the wide-angle PE model that can be used to simulate multilayer ocean media with high accuracy. In addition to a traditional pressure-release seabed, it is also capable of realistically modeling a rigid seabed without relying on an artificial absorbing layer. Waveguides that involve acoustic half-spaces are handled by utilizing the highly efficient PML technique, which significantly lowers the computational cost compared to the artificial absorbing layer approach.
- (2) The exponential convergence of spectral approximation guarantees the high precision offered by spectral methods. As a rule, spectral methods achieve greater accuracy than general difference schemes. Moreover,

- solving small-scale spectral matrices usually takes less time than solving finite difference matrices.
- (3) The new algorithm is well suited for simulating laterally inhomogeneous acoustic waveguides but is unable to accommodate topographic undulations in media, which is a significant limitation.

B. Summary

In this paper, a PE algorithm based on a spectral method is proposed, in which the Chebyshev spectral method is used to discretize a wide-angle parabolic model based on Padé rational approximation. For discontinuous layers in the depth direction, the Chebyshev–Tau spectral method is used to discretize them, and the resulting depth matrices are assembled in a diagonal block form to generate a global matrix. The number of subblocks in this global matrix corresponds to the number of layers of the media. The boundary and interface conditions are simultaneously incorporated into the linear equations. The proposed spectral algorithm has the ability to model both hard and soft seabeds through the imposition of distinct lower boundary conditions. Moreover, an acoustic half-space can be simulated by inserting a PML in the soft seabed. Remarkably, this PML can be treated as a standard layer during spectral discretization, without any special adjustments. Although its thickness is significantly less than that of a traditional artificial absorbing layer, its absorption effect is no less effective, and the computational cost is efficiently reduced. In each step of iteration, the algorithm checks whether the acoustic parameters of the media have changed. The inhomogeneity of the media is represented by updating the matrix \mathbf{X} . If there are no adjustments to the acoustic parameters, only multiplication of the transfer matrix is needed.

The computational speed advantage of spectral methods stems from the correspondingly smaller matrix size; however, the matrices formed via spectral discretization are also dense. Consequently, the sparsity of the global matrix is inferior to that of a finite difference matrix. The computational complexity of dense matrices is much higher than that of strip sparse matrices. Thus, for high-frequency waveguides, the speed advantage of SMPE will gradually weaken, and SMPE will eventually become slower than RAM, signifying a crossover point. Furthermore, the current algorithm can accommodate only inhomogeneous fluid media. In the future, the spectral model will be extended to the simulation of sound propagation in solid media, which will require the ability to simulate shear waves.

ACKNOWLEDGMENTS

The authors thank Dr. Chuanxiu Xu from Hangzhou Applied Acoustics Research Institute for his valuable guidance on the PML technique. This work was supported by the National Natural Science Foundation of China [Grant No. 61972406] and the National Key Research and Development Program of China [Grant No. 2016YFC1401800].

- ¹P. C. Etter, *Underwater Acoustic Modeling and Simulation* (CRC Press, Boca Raton, FL, 2018).
- ²F. B. Jensen, W. A. Kuperman, M. B. Porter, and H. Schmidt, *Computational Ocean Acoustics* (Springer-Verlag, New York, 2011).
- ³M. J. Buckingham, *Ocean-Acoustic Propagation Models* (Physics Editions, Les Ulis, France, 1992).
- ⁴F. T. Tappert, *The Parabolic Equation Approximation Method in Wave Propagation and Underwater Acoustics* (Springer, New York, 1977), Vol. 70.
- ⁵R. H. Hardin and F. D. Tappert, “Applications of the split-step Fourier method to the numerical solution of nonlinear and variable coefficient wave equations,” *SIAM Rev.* **15**, 423 (1973).
- ⁶J. A. Davis, D. White, and R. C. Cavanagh, “Parabolic equation workshop,” Naval Ocean Research and Development Activity, Stennis Space Center, MS (1982).
- ⁷R. R. Greene, “The rational approximation to the acoustic wave equation with bottom interaction,” *J. Acoust. Soc. Am.* **76**(6), 1764–1773 (1984).
- ⁸J. F. Claerbout, *Fundamentals of Geophysical Data Processing* (Blackwell, Oxford, 1985), pp. 2194–2207.
- ⁹M. D. Collins, “A higher-order parabolic equation for wave propagation in an ocean overlying an elastic bottom,” *J. Acoust. Soc. Am.* **86**(4), 1459–1464 (1989).
- ¹⁰M. B. Porter, F. B. Jensen, and C. M. Ferla, “The problem of energy conservation in one-way models,” *J. Acoust. Soc. Am.* **89**(3), 1058–1067 (1991).
- ¹¹M. D. Collins, “Higher-order Padé approximations for accurate and stable elastic parabolic equations with applications to interface wave propagation,” *J. Acoust. Soc. Am.* **89**(3), 1050–1057 (1991).
- ¹²M. D. Collins and E. K. Westwood, “A higher-order energy-conserving parabolic equation for range-dependent ocean depth, sound speed, and density,” *J. Acoust. Soc. Am.* **89**(3), 1068–1075 (1991).
- ¹³M. D. Collins, “An energy-conserving parabolic equation for elastic media,” *J. Acoust. Soc. Am.* **94**(2), 975–982 (1993).
- ¹⁴M. D. Collins, “A split-step Padé solution for the parabolic equation method,” *J. Acoust. Soc. Am.* **93**(4), 1736–1742 (1993).
- ¹⁵M. D. Collins, “Generalization of the split-step Padé solution,” *J. Acoust. Soc. Am.* **96**(1), 382–385 (1994).
- ¹⁶M. D. Collins, “A self-starter for the parabolic equation method,” *J. Acoust. Soc. Am.* **92**(4), 2069–2074 (1992).
- ¹⁷M. D. Collins, “The rotated parabolic equation and sloping ocean bottoms,” *J. Acoust. Soc. Am.* **87**(3), 1035–1037 (1990).
- ¹⁸M. D. Collins and D. K. Dacol, “A mapping approach for handling sloping interfaces,” *J. Acoust. Soc. Am.* **107**(4), 1937–1942 (2000).
- ¹⁹M. D. Collins and W. Siegmann, *Parabolic Wave Equations with Applications* (Springer, Berlin, 2019).
- ²⁰M. D. Collins, “User’s guide for RAM versions 1.0 and 1.0p” (1999), <https://oalib-acoustics.org/models-and-software/parabolic-equation/> (Last viewed June 6, 2022).
- ²¹M. D. Collins, “User’s guide for ram versions 1.0 and 1.0p,” Naval Research Laboratory Washington, DC (2006).
- ²²D. Gottlieb and S. A. Orszag, *Numerical Analysis of Spectral Methods, Theory and Applications* (Society for Industrial and Applied Mathematics, Philadelphia, PA, 1977).
- ²³B. Guo, *Spectral Methods and Their Applications* (World Scientific, Singapore, 1998).
- ²⁴J. P. Boyd, *Chebyshev and Fourier Spectral Methods*, 2nd ed. (Dover, New York, 2001).
- ²⁵J. Shen, T. Tang, and L. Wang, *Spectral Methods Algorithms, Analysis and Applications* (Springer-Verlag, Berlin, 2011).
- ²⁶C. Canuto, M. Y. Hussaini, A. Quarteroni, and T. A. Zang, *Spectral Methods Fundamentals in Single Domains* (Spring-Verlag, Berlin, 2006).
- ²⁷Y. Wang, H. Tu, W. Liu, W. Xiao, and Q. Lan, “Two Chebyshev spectral methods for solving normal modes in atmospheric acoustics,” *Entropy* **23**, 705 (2021).
- ²⁸M. A. Dzieciuch, “aw: A Matlab code for computing normal modes based on Chebyshev approximations” (1993), <https://oalib-acoustics.org/models-and-software/normal-modes/> (Last viewed June 6, 2022).
- ²⁹M. A. Dzieciuch, “Numerical solution of the acoustic wave equation using Chebyshev polynomials with application to global acoustics,” in *Proceedings of Oceans, IEEE*, Victoria, BC, Canada (1993), pp. 267–271.
- ³⁰R. B. Evans, “rimLG: A Legendre–Galerkin technique for differential eigenvalue problems with complex and discontinuous coefficients, arising

- in underwater acoustics" (2020), <https://oalib-acoustics.org/models-and-software/normal-modes/> (Last viewed June 6, 2022).
- ³¹H. Tu, Y. Wang, Q. Lan, W. Liu, W. Xiao, and S. Ma, "A Chebyshev–Tau spectral method for normal modes of underwater sound propagation with a layered marine environment," *J. Sound Vib.* **492**, 115784 (2021).
- ³²H. Tu, Y. Wang, Q. Lan, W. Liu, W. Xiao, and S. Ma, "Applying a Legendre collocation method based on domain decomposition to calculate underwater sound propagation in a horizontally stratified environment," *J. Sound Vib.* **511**, 116364 (2021).
- ³³R. Sabatini and P. Cristini, "A multi-domain collocation method for the accurate computation of normal modes in open oceanic and atmospheric waveguides," *Acta Acust. Acust.* **105**, 464–474 (2019).
- ³⁴H. Tu, "NM-CT: A Chebyshev–Tau spectral method for normal modes of underwater sound propagation with a layered marine environment in Matlab and Fortran" (2020), <https://oalib-acoustics.org/models-and-software/normal-modes/> (Last viewed June 6, 2022).
- ³⁵H. Tu, "MultiLC: A Legendre collocation method based on domain decomposition to calculate underwater sound propagation in a horizontally stratified environment in Matlab and Fortran" (2021), <https://oalib-acoustics.org/models-and-software/normal-modes/> (Last viewed June 6, 2022).
- ³⁶H. Tu, Y. Wang, C. Yang, W. Liu, and X. Wang, "A Chebyshev–Tau spectral method for coupled modes of underwater sound propagation in range-dependent ocean environments," *Phys. Fluids* **35**(3), 037113 (2023).
- ³⁷H. Tu, Y. Wang, C. Yang, X. Wang, S. Ma, W. Xiao, and W. Liu, "A novel algorithm to solve for an underwater line source sound field based on coupled modes and a spectral method," *J. Comput. Phys.* **468**, 111478 (2022).
- ³⁸H. Tu, Y. Wang, W. Liu, C. Yang, J. Qin, S. Ma, and X. Wang, "Application of a spectral method to simulate quasi-three-dimensional underwater acoustic fields," *J. Sound Vib.* **545**, 117421 (2023).
- ³⁹H. Tu, Y. Wang, Y. Zhang, H. Liao, and W. Liu, "Parallel numerical simulation of weakly range-dependent ocean acoustic waveguides by adiabatic modes based on a spectral method," *Phys. Fluids* **35**(1), 017119 (2023).
- ⁴⁰H. Tu, Y. Wang, W. Liu, S. Ma, and X. Wang, "A spectral method for the depth-separated solution of a wavenumber integration model for horizontally stratified fluid acoustic waveguides," *Phys. Fluids* **35**(5), 057127 (2023).
- ⁴¹D. Lee, G. Botseas, and J. S. Papadakis, "Finite-difference solution to the parabolic wave equation," *J. Acoust. Soc. Am.* **70**(3), 795–800 (1981).
- ⁴²S. T. McDaniel and D. Lee, "A finite-difference treatment of interface conditions for the parabolic wave equation: The horizontal interface," *J. Acoust. Soc. Am.* **71**(4), 855–858 (1982).
- ⁴³M. D. Collins, R. J. Cederberg, D. B. King, and S. A. Chin-Bing, "Comparison of algorithms for solving parabolic wave equations," *J. Acoust. Soc. Am.* **100**(1), 178–182 (1996).
- ⁴⁴K. E. Gilbert, "A finite element method for the parabolic wave equation," *J. Acoust. Soc. Am.* **69**(S1), S69 (1981).
- ⁴⁵D. Huang, "Finite element solution to the parabolic wave equation," *J. Acoust. Soc. Am.* **84**(4), 1405–1413 (1988).
- ⁴⁶Y. Wang, H. Tu, W. Liu, W. Xiao, and Q. Lan, "Application of a Chebyshev collocation method to solve a parabolic equation model of underwater acoustic propagation," *Acoust. Australia* **49**, 281–291 (2021).
- ⁴⁷H. Tu, Y. Wang, X. Ma, and X. Zhu, "Applying the Chebyshev–Tau spectral method to solve the parabolic equation model of wide-angle rational approximation in ocean acoustics," *J. Theor. Comput. Acoust.* **30**(2), 2150013 (2022).
- ⁴⁸H. Tu, Y. Wang, W. Liu, X. Ma, W. Xiao, and Q. Lan, "A Chebyshev spectral method for normal mode and parabolic equation models in underwater acoustics," *Math. Problems Eng.* **2020**, 7461314 (2020).
- ⁴⁹H. Tu, "SMPE: Two spectral methods for solving the range-independent parabolic equation model in ocean acoustics" (2021), <https://oalib-acoustics.org/models-and-software/parabolic-equation/> (Last viewed June 6, 2022).
- ⁵⁰R. B. Evans, "COUPLE: A coupled normal-mode code (Fortran)" (2007), <https://oalib-acoustics.org/models-and-software/normal-modes/> (Last viewed June 6, 2022).
- ⁵¹J. P. Berenger, "A perfectly matched layer for the absorption of electromagnetic waves," *J. Comput. Phys.* **114**(2), 185–200 (1994).
- ⁵²W. C. Chew and W. H. Weedon, "A 3-D perfectly matched medium from modified Maxwell's equations with stretched coordinates," *Microwave Opt. Technol. Lett.* **7**(13), 599–604 (1994).
- ⁵³D. Yevick and D. J. Thomson, "Impedance-matched absorbers for finite-difference parabolic equation algorithms," *J. Acoust. Soc. Am.* **107**(3), 1226–1234 (2000).
- ⁵⁴Y. Lu and J. Zhu, "Perfectly matched layer for acoustic waveguide modeling—benchmark calculations and perturbation analysis," *Comput. Modeling Eng. Sci.* **22**(3), 235–247 (2007).
- ⁵⁵M. S. Min and D. Gottlieb, "Domain decomposition spectral approximations for an eigenvalue problem with a piecewise constant coefficient," *SIAM J. Numer. Anal.* **43**, 502–520 (2005).
- ⁵⁶A. D. Chowdhury, C. P. Vendhan, S. K. Bhattacharyya, and S. Mudaliar, "A Rayleigh–Ritz model for the depth eigenproblem of heterogeneous Pekeris waveguides," *Acta Acust. Acust.* **104**, 597–610 (2018).
- ⁵⁷D. J. Thomson, G. H. Brooke, and J. A. DeSanto, "Numerical implementation of a modal solution to a range-dependent benchmark problem," *J. Acoust. Soc. Am.* **87**(4), 1521–1526 (1990).
- ⁵⁸M. B. Porter, *The Kraken Normal Mode Program*, SACLANT Undersea Research Centre (2001). <https://oalib-acoustics.org/models-and-software/normal-modes/> (Last viewed June 6, 2022).
- ⁵⁹M. A. Dzieciuch, "MATLAB RAM: A MATLAB version of RAM by Matt Dzieciuch with notes by (B. Dushaw, Applied Physics Laboratory, U. Washington)" (2015), <https://oalib-acoustics.org/models-and-software/parabolic-equation/> (Last viewed June 6, 2022).